Original Article

Movement of magnetic nanoparticles in brain tissue: mechanisms and impact on normal neuronal function

Bharath Ramaswamy, PhD candidate[a],[*], Sandip D. Kulkarni, PhD[a], Pablo S. Villar, BS[b],
Richard S. Smith, PhD[b], Christian Eberly, BS[b], Ricardo C. Araneda, PhD[b],
Didier A. Depireux, PhD[c], Benjamin Shapiro, PhD[a],[c]

[a]Fischell Department of Bioengineering, University of Maryland, College Park, MD, USA
[b]Department of Biology, University of Maryland, College Park, MD, USA
[c]The Institute for Systems Research (ISR), University of Maryland, College Park, MD, USA

Abstract

Magnetic nanoparticles (MNPs) have been used as effective vehicles for targeted delivery of theranostic agents in the brain. The advantage of magnetic targeting lies in the ability to control the concentration and distribution of therapy to a desired target region using external driving magnets. In this study, we investigated the behavior and safety of MNP motion in brain tissue. We found that MNPs move and form nanoparticle chains in the presence of a uniform magnetic field, and that this chaining is influenced by the applied magnetic field intensity and the concentration of MNPs in the tissue. Using electrophysiology recordings, immunohistochemistry and fluorescent imaging we assessed the functional health of neurons and neural circuits and found no adverse effects associated with MNP motion through brain tissue.

From the Clinical Editor: Much research has been done to test the use of nanocarriers for gaining access across the blood brain barrier (BBB). In this respect, magnetic nanoparticles (MNPs) are one of the most studied candidates. Nonetheless, the behavior and safety of MNP once inside brain tissue remains unknown. In this article, the authors thus studied this very important subject.
© 2015 Elsevier Inc. All rights reserved.

Key words: Magnetic nanoparticles; Transport; Drug delivery; Brain; Safety

Nanotechnology based solutions for the treatment of brain tumors have been developed in recent years to address the challenges faced by conventional cancer therapeutics[1] such as surgery,[2,3] chemotherapy[4–6] and radiation therapy.[7,8] Drugs such as doxyrubicin[9] and oxantrazole[10] can be combined with appropriate nanocarriers to penetrate the blood brain barrier (BBB) to increase the intracellular concentration of drugs in tumor cells.[11–13] Magnetic nanoparticles (MNPs) have been investigated as effective nanocarriers for targeted drug delivery in the brain.[14–17] MNPs coated with pharmacological agents, proteins, and genes can potentially be imaged using MRI technology and guided toward brain tumor locations using external magnets.

MNPs with an aminosilane coating have been investigated in human trials for targeting glioblastoma multiforme cells and have been shown not to cause any adverse effects in patients. In the presence of an alternating magnetic field, the MNPs were found to extend tumor necrosis with minor or no side effects in the patients.[17] Hassan and Gallo showed that after a systemic injection of magnetic chitosan microspheres coated with oxantrazole, while in the presence of a 0.6 T magnetic field, microspheres accumulated in a targeted region of rat brain tissue.[10] Thus, MNPs have been shown to cross the BBB and reach targets in brain tissue without disrupting the barrier in rat models.[15,18]

Furthermore, endothelial progenitor cells (EPCs) from humans have been loaded with MNPs and guided to targets in mouse brains.[19] These EPCs loaded with MNPs have shown increase in secretion and migration of growth factors such a vascular endothelial growth factor (VEGF) and fibroblast growth factor

(FGF), in vitro, thereby promoting angiogenesis for neural regeneration. Various in vitro studies have shown that cancer cells can be made to internalize a higher level of nanoparticles with drugs by appropriate targeting of receptors.[20–23] This illustrates that MNPs can be used as a potential option to circumvent the challenges faced by conventional drug delivery techniques.

Most of the work mentioned above has focused on the motion of MNPs through blood vessels and the observation of MNP presence in living tissue.[15,24,25] The motion of MNPs in brain tissue surrounding the blood vessels is expected to differ from its motion in the vessels. Hence there is a need for a better understanding of the motion of MNPs in brain tissue after extravasating from blood vessels. To be appropriate for therapeutic purposes, MNP movement cannot induce cytotoxic effects, nor should it adversely influence circuit function. Addressing these needs will result in better nanotherapeutic schemes to target tumors in brain tissue diminishing permanent side effects following drug delivery.

Here, we examine the movement MNPs in brain tissue under an applied magnetic field. The movement of MNPs throughout this work includes the interactive motion of MNPs toward each other caused by the influence of an external magnetic field. Using whole-cell patch recordings, immunohistochemical staining and confocal imaging, we found that the motion of MNPs did not cause any detrimental effects on the functional health of the neurons or the circuit function in the main olfactory bulb.

Methods

Characterization of magnetic nanoparticles

The physical properties (mean hydrodynamic diameter, polydispersity index) of MNPs (nano-screenMag, Chemicell, listed as 300 nm diameter) used in our experiments were determined using dynamic light scattering. The MNPs were required to be monodispersed to avoid non-uniformity in their motion in the tissue caused by particle size variations. For the dynamic light scattering measurements, the stock concentration of MNPs (25 mg/mL in double distilled water) was diluted with de-ionized water to a concentration of 0.25 mg/mL. Three samples of 3 mL of the diluted solution were used for the measurement assays. The particle size distribution curve was plotted for these samples and used to calculate the polydispersity index (Figure 1, *A* in Supplementary materials).

The magnetic properties of the nanoparticles including magnetic susceptibility and saturation magnetization were measured using a vibrating sample magnetometer (Lake Shore Cryotronics Inc.). Sample volumes of 60 µL of MNPs in DI water were pipetted into the sample holder (Kel-F) and the holder was placed in the vibrating sample magnetometer setup. The experiments were performed at room temperature (298 K). The samples were exposed to a cycle of different magnetic field values in the range of −1.5 to +1.5 tesla and the corresponding net magnetization produced in the samples was recorded. The magnetic properties (susceptibility and saturation magnetization) of the samples were then calculated from the magnetization versus magnetic field (M vs H) plot obtained from the vibrating sample magnetometer (Figure 1, *B* in Supplementary materials).

Uniform magnetic field using a two magnet setup

A system was created to apply a uniform magnetic field to magnetic nanoparticles inside brain tissue slices. A uniform magnetic field was desired so that all MNPs in the tissue would experience the same magnetic field irrespective of their location in the tissue. Two permanent magnets, appropriately sized and placed as shown in Figure 1, *A*, were sufficient to create a uniform magnetic field. The uniformity of the field was verified by a 3-channel Gaussmeter (Lake Shore Inc.) mounted on a piezo positioning stage (VXM Motor Inc.). The Gaussmeter measured the spatial distribution of the magnetic field intensity between the two magnets and it was found that the deviation from the mean magnetic field intensity in the tissue sample volume was less than 1%. These data are displayed in Figure 2 in the Supplementary Materials.

Motion of MNPs in the brain slices

The motion of MNPs toward each other under the influence of an applied uniform magnetic field was studied in rat brain slices using a total of 12 rats (Sprague Dawley). Each different motion experiment was repeated three times using tissue from different rats to ensure that the data were independent of animal to animal variability. The rat brains were dissected out and immediately stored at 4 °C in 1X Phosphate Buffer Saline (PBS) solution to increase their viability. After 15 minutes, the brains were injected in the prefrontal cortex with 4 µL of the MNPs, using a 10 µL micro-syringe (Hamilton). Following this injection we obtained cortical slices using a razor blade. The slicing was facilitated by the low temperature storage of the brain samples. The slices containing the injected MNPs were then stabilized at room temperature in 1X PBS solution in a Petri dish. The MNPs were visualized by fluorescence using a lipophilic dye coating (Texas Red, Chemicell) with excitation and emission wavelengths of 578 nm and 613 nm respectively. The Petri dish containing the brain slices, immersed in PBS, was placed in the uniform magnetic field region of the two magnet setup. The effect of the uniform magnetic field on the MNPs in the brain slices was observed using a fluorescence microscope (Zeiss) with ×40 magnification and recorded using a video camera (Hamamatsu). The videos were post-processed in MATLAB (Mathworks) to quantify the movement of the MNPs in the uniform magnetic field.

Electrophysiological recordings

All animal studies were conducted in accordance with the policies and recommendations of the National Institute of Health Guide for the Care and Use of Laboratory Animals, and under approval from the Institutional Animal Care and Use Committee of the University of Maryland. The electrophysiological recordings were performed in brain slices extracted from wild-type BL6/C57 mice (Jackson Labs), or 4-6-week-old transgenic mice expressing green fluorescent protein (GFP) and subjected to MNP motion. Specifically, we used the ChAT-Tau-GFP line, generously provided by Dr. Sukumar Vijayaraghavan.[26] We performed these electrophysiology experiments in mice because of the feasibility of transgenic modification in a mouse model compared to a rat model. All the functional experiments involved whole-cell
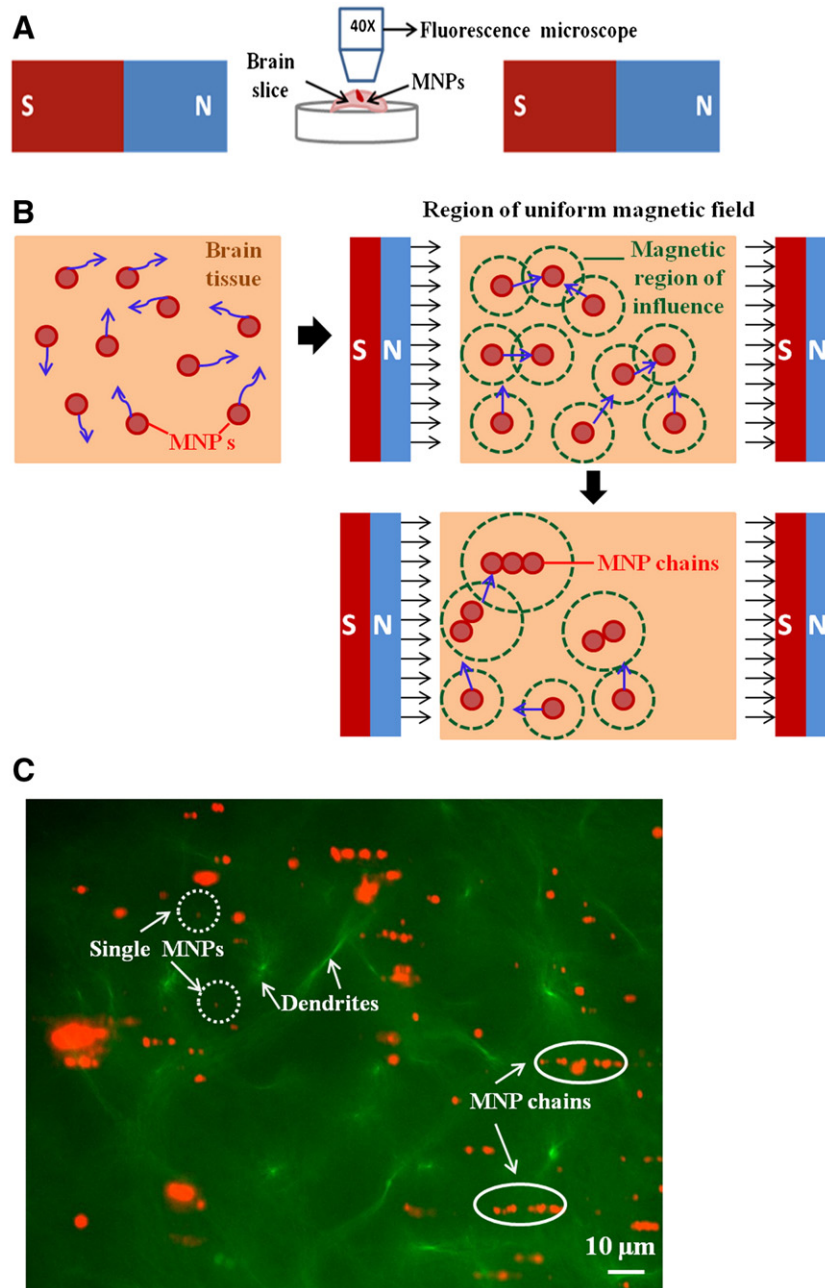
Figure 1. **(A)** The diagram of two-magnet setup used to study movement of MNPs in brain tissue. The tissue loaded with MNPs was mounted and visualized under a fluorescence microscope after exposing it to the uniform magnetic field **(B)** An illustration of how MNPs behave in brain tissue with and without an applied uniform magnetic field. The MNPs diffuse in different directions (blue arrows) in the absence of a uniform magnetic field (left, top). After the introduction of the magnetic field, the MNPs move toward each other due to an overlap of induced magnetic fields of influence (green circles). As a result, the MNPs form chains as they move toward each other and longer chains have a larger field of influence which recruits additional particles to the chain (bottom). **(C)** Chaining of MNPs experimentally observed in mouse brain tissue (pre-frontal cortex region) in the presence of a uniform magnetic field. The MNP chains (orange) and the barely-visible single MNPs are marked by white ovals and white dotted circles respectively. The dendrites (green) in the tissue are indicated by white arrows.

patching of neurons in an electrophysiology setup. The transgenic modification of mice enabled us to visualize the GFP expressing neurons in the presence of MNPs around them using a fluorescence microscope with multiple wavelength filters. Neurons from at least 5 different brains were used for the studies. The animals were anesthetized with isofluorane and decapitated. The whole brain was removed and immediately placed in ice-cold oxygenated artificial cerebrospinal fluid (ACSF). The ACSF used for the experiments contained the following composition (in mM): 125 NaCl, 25 NaHCO$_3$, 1.25 NaH$_2$PO$_4$, 3 KCl, 2 CaCl$_2$, 1 MgCl$_2$, 3 myo-inositol, 0.3 ascorbic acid, 2 Na-pyruvate, and 15 glucose. The solution was maintained at a constant pH of 7.4 and osmolarity of ~350 mOsm by continuous oxygenation (95% O$_2$- 5% CO$_2$). A block of the extracted tissue, containing the olfactory bulb, was

glued to a stage with cyanoacrylate and bathed in ice-cold low Ca^{2+}, high Mg^{2+} ACSF. Sagittal brain sections (250-300 μm), containing the olfactory bulb were sliced using a vibratome slicer (Leica). The slices were held at 34 °C for 30 minutes and then at room temperature to recuperate.

The slices were then transferred to a Petri dish and the MNPs were injected into the slices using a glass micro-pipette (≈ 5 μm diameter) attached to a micro injection system (Toohey spritzer). The MNPs in the brain slice were visualized using a fluorescence microscope and the two magnet setup was introduced for 5 minutes to produce MNP motion and chaining. Then the two magnet system was rotated by 90° to produce motion of MNPs in a perpendicular direction to ensure that the functional safety of neurons did not depend on the direction of MNP movement. The slices were then placed in the electrophysiology recording chamber mounted on the stage of an upright fluorescence microscope (Zeiss) and the region of the tissue containing MNPs was identified using fluorescence. Then neurons in that region were patched for electrophysiology recordings. The recordings were carried out in current-clamp and voltage-clamp mode using standard patch pipettes (3-7 MΩ resistance) pulled on a horizontal puller (Sutter). To further assess neuronal integrity and viability in slices loaded with MNPs, after the application of a magnetic field, we included the fluorescent dye Alexa-Fluor 488 (10 μM, Life Technologies) in the recording pipette solution. Data were acquired using a dual EPC10 amplifier (HEKA) and analyzed offline using the IgorPro software (Wavemetrics). We conducted control experiments in slices obtained from the same brain but not injected with MNPs or injected with the MNPs but not subjected to the magnetic field.

Calcium imaging

Following the post-slicing recuperation period, slices were transferred to a 30 mm Milicell culture dish insert (Millipore Corp, Billerica, Ma) containing 5 mL of normal oxygenated ACSF with 5 μM freshly prepared Fluo-4 AM Pluronic Acid F-127 20% solution in DMSO (Molecular Probes, Life Technologies). Slices were submerged in the dye for 20 minutes then transferred to a submerged recording chamber mounted on the stage of an Olympus BX51 microscope for acquisition.

We visualized labeled slices using epifluorescence illumination and a ×40 water immersion objective. Illumination was achieved using an OPTOLED green LED (exciter 488 nm center wavelength, Chroma; Cairn Research LTD), emitted light was collected by an ORCA-Flash4.0 V2 sCMOS camera (Hamamatsu), and images were recorded using the HCimage software (Hamamatsu). Imaging analysis was performed offline using the ImageJ and IgorPro (Wavemetrics) softwares. (S)-1-Aminopropane-1,3-dicarboxylic acid (Glutamate) was prepared from a stock solution and added to the bathing solution. The calcium indicator, Fluo-4 AM (Molecular Probes, Life Technologies), was excited at a wavelength of ~490 nm and the resulting emission detected at ~520 nm. The optical recording data are shown as the ratio of the change in fluorescence caused by glutamate in cells after 60 seconds to the baseline fluorescence ($\Delta f/f_0$) for the indicated regions of interest.

Immunohistochemistry

The ex-vivo brain slices from ChAT-tau-GFP mice were analyzed using immunohistochemistry after magnetic field induced MNP motion. The nerve fibers in the slices were visualized using anti-GFP immunostaining to assess any damage caused due to MNP movement. The slices were extracted as above, injected with MNPs in the main olfactory bulb, and exposed to a uniform magnetic field in two different directions as described in the previous section. The slices were then fixed in 4% paraformaldehyde for 5 minutes, transferred to saline solution at 4 °C, and then quickly washed with 1X PBS for 2 minutes. The slices were then incubated with the blocker (10% Donkey serum in PBS-T) for 1 hour, followed by incubation with the primary antibody in 2.5% donkey serum in PBS-T overnight at room temperature. The slices were then washed once in PBS-T and then 7 × for 5 minutes each in PBS-T and incubated in the secondary Alexa-488 antibody solution (1:750 concentration) for 2 hours at room temperature. Then, the slices were washed 3 × for 5 minutes in PBS-T, then further rinsed 3 × for 5 minutes each in PBS. At this point, immunostained slices were visualized using confocal microscopy with appropriate fluorescence filters for the MNPs and the GFP-stained fibers.

Results

The MNPs were analyzed using dynamic light scattering to calculate the particle size distribution and the extent of polydispersity. The mean hydrodynamic diameter of the samples was measured to be 274.6 ± 40 nm (n = 3 samples) with a polydispersity index of 2%. The distribution of hydrodynamic diameter in the samples is shown in Supplementary Figure 1, *A*. The magnetization of the particles was measured using the vibrating sample magnetometer for different field intensities and the hysteresis curve for the MNPs is shown in Supplementary Figure 1, *B*. The saturation magnetization of the particles was calculated to be 0.06 emu at a saturating magnetic field of 0.5 T. The magnetic susceptibility of the nanoparticles was calculated from the M vs H plot and was found to be χ_m = 15.2. Based on these measurements, the MNPs exhibited superparamagnetic behavior and were confirmed to be monodispersed.

The movement of MNPs was examined in rat and mouse cortical brain slices under a uniform magnetic field Figure 1, *A*. These ex-vivo cortical slices were maintained at a low temperature in order to preserve structure and extend sample viability. Prior to applying a magnetic field, the MNPs diffused in random directions in the tissue. However, when the uniform field was applied to the tissue using the two magnet system, each magnetized MNP produced a magnetic field of influence around it. An MNP falling in the field of influence of any neighboring MNP experiences an attractive magnetic force toward its neighbor.[27] This attractive force between particles causes the motion of MNPs toward their neighbors. The interactive motion of MNPs in the presence of a uniform magnetic field resulted in the formation of MNP chains. Figure 1, *C* shows a representative image of this chaining of MNPs in a mouse brain slice (GFP line) after the application of a magnetic field. The MNP chains increased in size over time as new particles were recruited to the chain and as the corresponding region of the

Table 1
Average chain length after 10 minutes for different combinations of applied magnetic field intensity and MNP concentration in rat brain tissue (n = 12).

MNP Concentration Magnetic Field	High Concentration (0.5 mg/mL)	Low Concentration (0.05 mg/mL)
High field (0.1 T)	12.51 ± 3.5 µm	5.84 ± 1.1 µm
Low field (0.02 T)	2.76 ± 0.8 µm	No Chaining

magnetic field of influence grew larger. The phenomena of movement and agglomeration of MNPs into chains were observed in all slices from different animals.

The motion of MNPs was further evaluated in rat brain slices after varying two key parameters in the above experiment, namely, magnetic field intensity and MNP volume concentration. The experiments were performed by combining either high (0.1 T) or low (0.02 T) uniform magnetic field intensity with either high (0.5 mg/mL) or low (0.05 mg/mL) MNP concentration. Each of these four experiments was repeated over three slices from different rats. In 3 out of the 4 experiments, MNPs formed chains in the presence of a uniform magnetic field while in one case, at a low magnetic field and low magnetic concentration, the MNPs were too far apart and the magnetic field was too small to produce any chaining. Table 1 lists a comparison of the extent of chaining observed for each combination of parameters. The amount of chaining for each of the experiments was defined by the average MNP chain length observed in the tissue after 10 minutes of applying the uniform magnetic field. As anticipated, the largest MNP chaining was observed for a combination of high magnetic field and high magnetic concentration (12.51 ± 3.5 µm). In addition, the chain length observed in a high magnetic field and low MNP concentration (5.84 ± 1.1 µm) was higher than observed for the case of a low magnetic field and a high MNP concentration (2.76 ± 0.8 µm). This indicated a dominant effect of magnetic field intensity over the MNP concentration in the process of MNP movement and chaining.

To determine the functionality of cells after moving MNPs through or near them, we performed standard electrophysiology recordings in the neurons of the olfactory bulb in mice.[28,29] Mitral cells from the main olfactory bulb were targeted for whole-cell recordings, after moving MNPs through a region that contained those cells. In these experiments the recording pipette contained a fluorescent dye (see methods), which allowed us to visually verify the integrity of the recorded neuron. As shown in Figure 2, B, following the movement of MNPs, mitral cells remain excitable as determined by current injections, indicating that basic processes such as influx and efflux of sodium and potassium ions[30] respectively were unaffected by the motion of MNPs. The motion of MNPs did not alter the dependence of neuron firing frequency for different constant currents injected into the cells (Figure 2, C). Additionally, we tested synaptic functionality by examining the occurrence of spontaneous inhibitory post-synaptic currents (sIPSCs) in mitral cells. Previously, it had been shown that noradrenaline, a neuromodulatory transmitter, enhances the release of gamma-aminobutyric acid (GABA) from granule cells in the main olfactory bulb, and

greatly enhances the frequency of spontaneous inhibitory post-synaptic currents in mitral cells.[31] As shown in Figure 3, B, slices exposed to noradrenaline (NA, 10 µM, for 3 minutes) after MNP motion showed a significant increase in spontaneous inhibitory post-synaptic current frequency, suggesting that the synaptic connectivity between granule and mitral cells in the main olfactory bulb remained functional.

Next, we assessed whether the magnetically induced movement of MNPs disrupted the neural circuit function in the olfactory bulb. The olfactory bulb has a well-characterized neural circuit in which sensory inputs excite principal neurons, specifically the mitral/tufted cells.[32] Activation of mitral cells then excites the surrounding granule cells at dendrodendritic synapses. Thus, by monitoring the granule cells after MNP movement, we studied the effect of MNP motion on the excitatory synapses in the olfactory bulb.[32] To investigate olfactory bulb neural circuit function, we loaded olfactory bulb slices with a Ca^{2+} sensing dye (Fluo-4 AM dye, 5 µM, see Methods) to visualize and monitor the neural activity of the circuit, in particular granule cells (the most abundant neuron in the olfactory bulb) (Figure 4, B). Fluo-4 dye AM is a cell permeable dye that exhibits an increase in fluorescence upon binding to Ca^{2+} (indicating neural activation), and allows for the monitoring of a large number of neurons simultaneously. MNPs were applied to the slice 30 minutes before the acquisition of images began and they were moved by exposure to a uniform magnetic field. We then assessed the responsiveness of granule cells to activation by the excitatory neurotransmitter glutamate after MNP movement in the region (Supplementary video 1). As shown in Figure 4, B, following the movement of MNPs in the slice, granule cells show normal fluorescence labeling suggesting that the overall morphology is maintained. In these slices, application of glutamate (100 µM) resulted in a robust increase in intracellular Ca^{2+} as evidenced by the changes in $\Delta F/F_0$ (45.25 ± 8.2%, n = 6 cells). Hence the responses to excitatory stimuli in granule cells were not affected by the MNP movement in the region.

To further determine whether the movement of MNPs disrupted neural connections, we used transgenic mice (ChAT Tau-GFP) that expressed GFP under the promoter of choline acetyl transferase (ChAT), an enzyme involved in the synthesis of acetylcholine. Since the main olfactory bulb receives a rich cholinergic projection from the basal forebrain,[33] we visualized the effect of MNPs on the fibers in this particular region. The slices used in these experiments were divided into three main categories: treated, untreated, and control. The treated slices were injected with MNPs and were subjected to the applied uniform magnetic field for 5 minutes, followed by a rotation of the field for 5 minutes as explained in the Methods section. The untreated slices were injected with MNPs, but were not exposed to a magnetic field. The control slices contained no MNPs and no magnetic field was applied. As shown in Figure 5, immunostaining of GFP in control mice samples (Figure 5, left) revealed abundant fiber expression in the granule cell layer of the main olfactory bulb. The untreated (Figure 5, middle) and treated slices (Figure 5, right) showed no difference in the pattern of distribution of GFP-positive fibers. Hence the motion or presence of MNPs did not disrupt the neural connections in the brain independent of the direction of MNP motion.
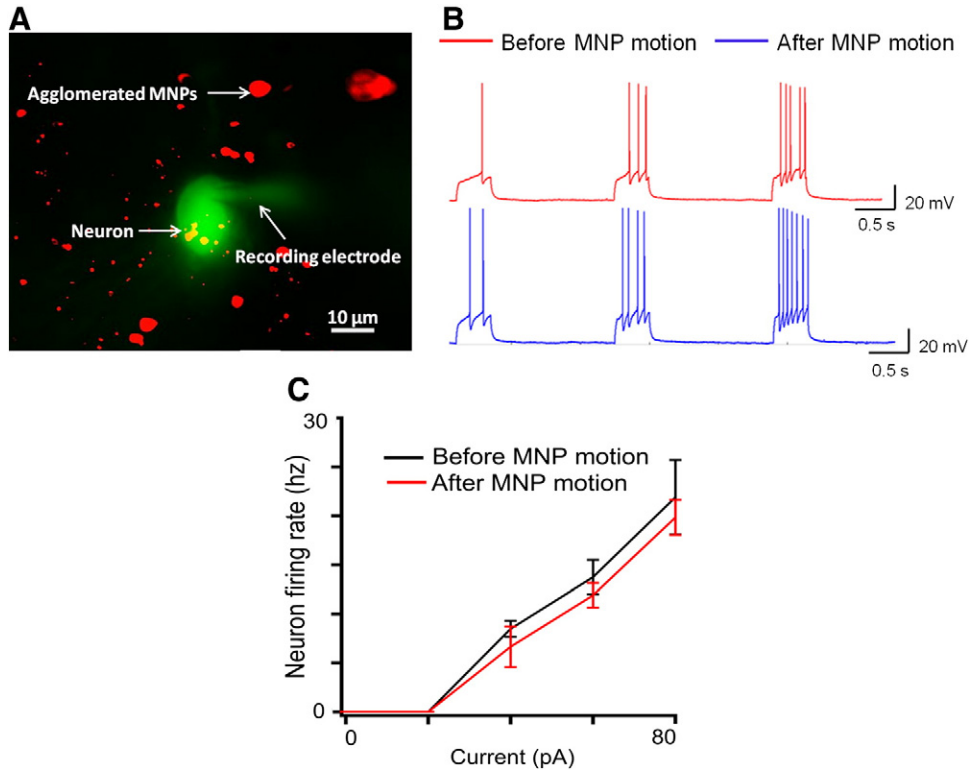
Figure 2. Functional health of brain tissue after MNP motion. **(A)** Recording from a mitral cell in the olfactory bulb after the slices treated with MNPs were subjected to a magnetic field. The recording electrode contained the fluorescent dye Alexa-488 (green), which diffuses into the neuron during the recording. The MNPs contained a fluorophore Texas-Red (red). Note this is a total summed two wavelength images **(B)**. Current-clamp recordings in mitral cells before (red) and after magnet induced MNP movement (blue). Increasing depolarizing current pulses (not shown) elicited action potentials in both control and treated neurons. **(C)** In the range of depolarizing current used, the frequency of neuronal firing increased linearly and it was comparable for different constant current stimuli before (black) and after MNP motion (red).
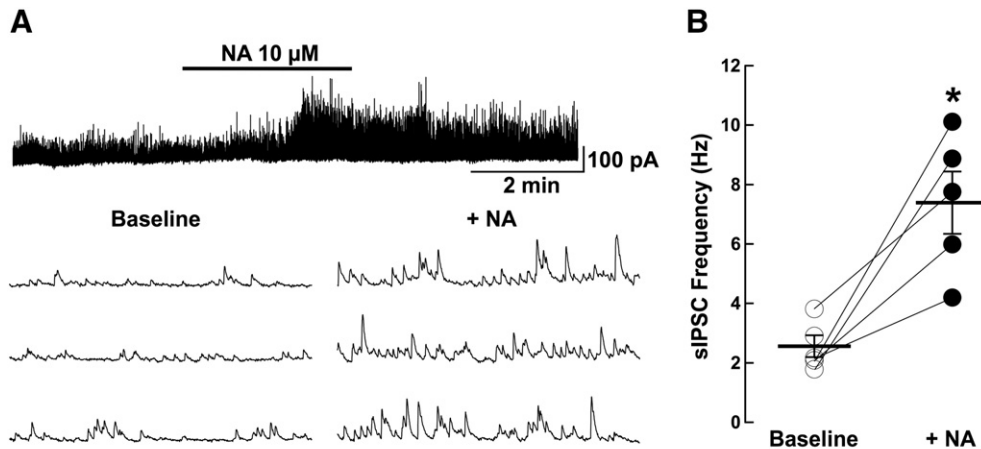

Figure 3. Synaptic connectivity in the olfactory bulb after MNP motion **(A)** Recording from a mitral cell showing the spontaneous occurrence of GABA IPSCs after MNP motion in brain slices. Top, application of noradrenaline (NA, 10 μM, 3 min) produced a long lasting increase in sIPSC frequency in this cell. Bottom, select traces from above, in an expanded time scale, showing sIPSC before (left) and after NA (right). **(B)** NA significantly increased the sIPSC frequency; baseline, 2.56 ± 0.82 Hz, NA, 7.39 ± 2.34 Hz (*, $P < 0.003$; n = 5). The observed increase in sIPSC frequency caused by NA after MNP motion is similar to the trend observed previously by Zimnik et al.[31]

Discussion

In previous works, MNPs of various sizes, shapes, and coatings have been successfully utilized in drug delivery, gene transfection, tumor imaging, and regenerative medicine.[16,18,34–36] In principle, such MNPs can be controlled in the human body using external magnet systems to direct drugs and other biological factors to specific targets. Here we examined the motion of MNPs in brain
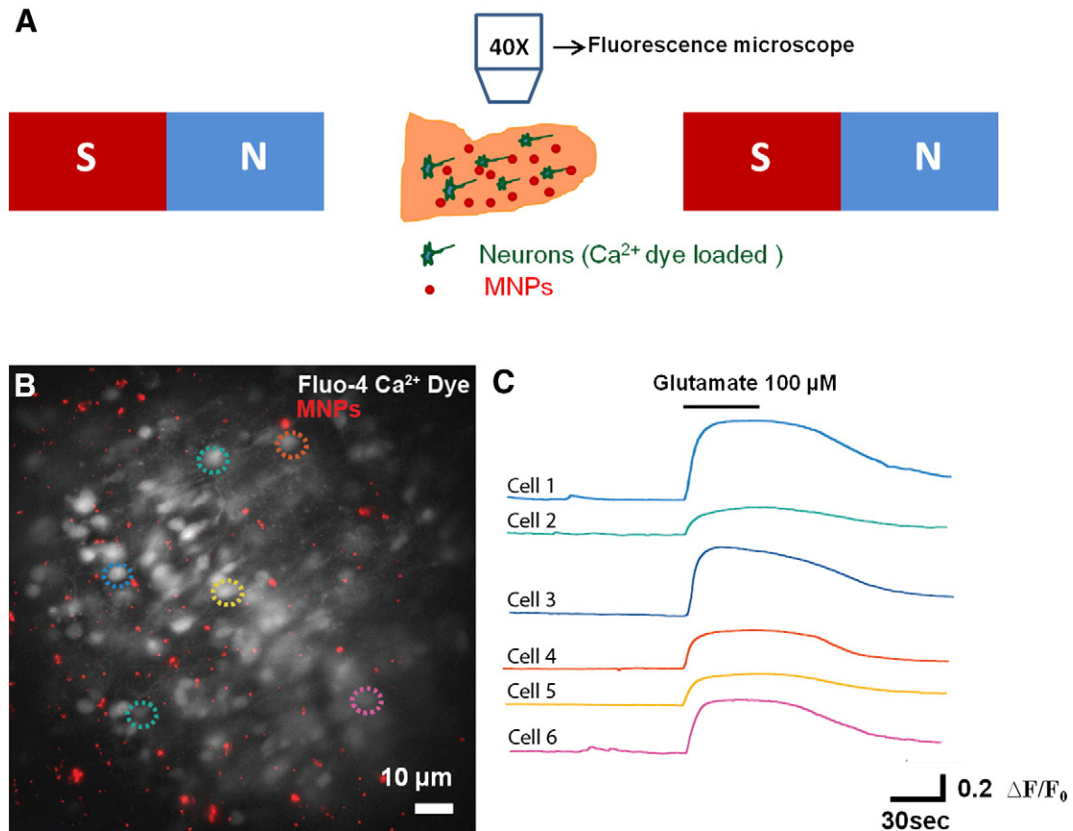
Figure 4. Calcium imaging recording in brain slices after MNP motion. **(A)** Experimental setup used for the calcium imaging experiments. After loading the calcium dye, MNPs are placed on the slice and subjected to a magnetic field. **(B)** Fluorescence image showing a network of functionally active neurons in a brain slice loaded with the calcium dye Fluo-4 AM (white) and MNPs (red), after exposing the slice loaded with MNPs to a uniform magnetic field. Dotted colored circles represent the neurons used for quantification of fluorescence changes shown on the right. **(C)** Optical fluorescence recordings of the selected cells shown in B. Images were taken at a rate of 1 Hz FPS. Application of the excitatory neurotransmitter, glutamate (100 μM, 45 seconds) resulted in a large, and reversible, increase in intracellular calcium levels. The color of each plot corresponds to cells indicated by the colored dotted circles in **(B)**.

tissue, to investigate both the character of MNP motion in the brain and its safety. We showed that monodispersed starch-coated MNPs are able to move toward each other in brain slices when exposed to a uniform magnetic field and, importantly, that this movement produced no apparent disruption of the neural circuit function in the olfactory bulb.

We observed that the MNPs agglomerated into chain like structures as they moved in the brain tissue under the influence of a uniform magnetic field. Such an agglomeration of MNPs in a uniform magnetic field has been previously studied in various media such as in water, bovine serum albumin and sodium dodecyl sulphate.[37,38,27] The dynamics of chain formation and the distribution of chain length have been modeled and compared with experiments.[38–40] Based on these prior studies, the mechanism of chain formation can be classified into two main cases: diffusion dominated and magnetic drift dominated agglomeration. In diffusion dominated agglomeration, the MNPs undergo diffusion in the media until they are close enough so that they bring each other together by the magnetic forces between them.[41–43] In the drift dominated agglomeration, the magnetic force has a sufficiently long range that it drives the motion of MNPs together from the start.[44–46] In our experiments in brain tissue, the average chain length of MNPs was higher in a high magnetic field and low MNP concentration than in a low magnetic field and high concentration condition. This

indicates that a high magnetic field intensity can bring even sparsely distributed nanoparticles together. Thus for our experimental conditions, the MNPs exhibit a magnetic drift dominated mechanism of agglomeration as they moved in brain tissue.

The MNPs used in this work have been shown not to produce cytotoxicity in various cell types and in-vivo studies.[13,47,48] However, it is equally important to study and ascertain that the motion of these nanoparticles in the brain does not affect the normal function of neurons or their connectivity. By taking electrophysiological recordings of neurons before and after MNP movement, we have shown that the MNP motion and chaining did not affect neural functionality. Current injections produced a robust depolarization in the neurons, and they exhibited a stimulus-dependent increase in firing when a constant current stimulus was provided to the cell. Importantly, the change in neural firing rate elicited by incremental current stimuli was not affected by the MNP motion. Therefore, we conclude that MNP presence, motion, or chaining did not affect the physiological properties of neurons.

In addition, we showed that the movement of MNPs did not affect the inhibitory neural circuit in the olfactory bulb; a critical component of olfactory processing. The frequency and amplitude of the GABA sIPSCs after movement of the MNPs were similar to the previously reported values.[31] Further, since the sIPSCs recorded in the mitral cells are produced by the summation of
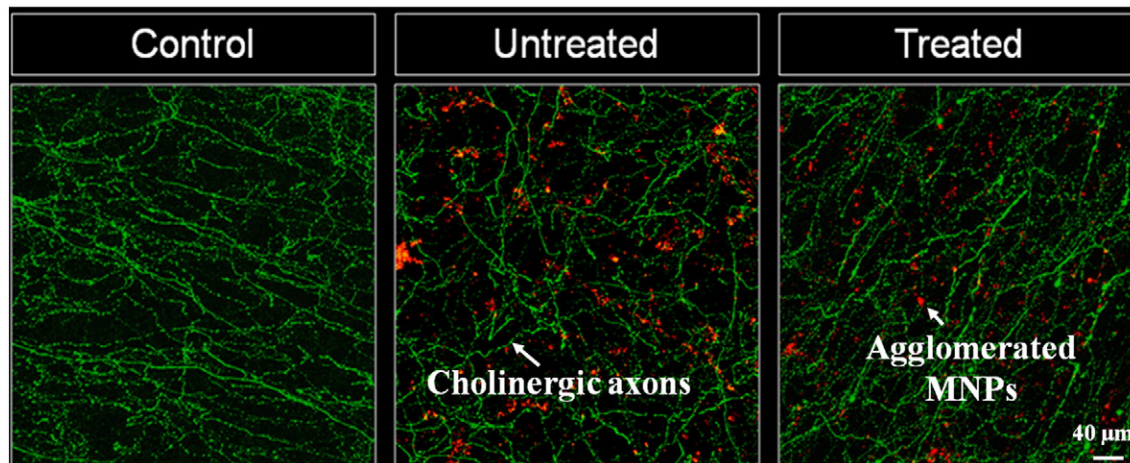
Figure 5. Confocal microscopy images of the granule cell layer in the main olfactory bulb from ChAT-Tau-GFP mice, after immunostaining for GFP. In control conditions (left) the slices show abundant distribution of GFP labeled fibers, corresponding to the axonal processes of cholinergic neurons. The pattern of distribution of axonal fibers was not affected in slices treated with MNPs without application of the magnetic field (middle) or after the MNPs exhibited motion into chains under an applied uniform magnetic field (right).

multiple synapses from several interneuron types, these results suggest that circuit level basal release from interneurons and post synaptic mitral cells activation was not affected following MNP motion. Furthermore, noradrenaline caused a large increase in the spontaneous inhibitory post-synaptic current frequency in mitral cells, suggesting that the overall functionality of interneurons was also not affected by the MNPs movement (see also Zimnik et al.[31]). This conclusion was further supported by the analysis of excitatory glutamatergic responses in a population of granule cells using a calcium indicator. In these optical recordings we found that a wide field of granule cells showed an increase in fluorescence after exposure to glutamate despite MNP motion in the same region (Supplementary video 1). The increase in fluorescence corresponds to an increase in intracellular calcium ions in the granule cells, in response to the glutamate-induced excitation. Together, these results provide evidence that excitatory and inhibitory responses of the olfactory bulb neural network were not affected by the MNP movement.

Apart from the physiological health of the neurons, the immunohistochemistry suggested that the MNPs did not disrupt the fibers as they moved and chained in the tissue. The slices containing MNPs (both with and without an applied uniform magnetic field) did not exhibit any noticeable difference in the density of cholinergic fibers in the granule cell layer, as compared with the control slices with no MNPs and no applied magnetic field. These experiments ruled out the possibility that the passive diffusion or magnetically induced movement of MNPs disrupted neural connections.

In summary, we have shown that MNPs can move toward each other in brain tissue under an applied uniform magnetic field. This motion of MNPs results in the formation of chain like agglomerates in the tissue and for our experimental conditions this chaining was determined to be drift dominated (as opposed to diffusion dominated) behavior. We found that the chained MNP agglomerates did not affect the normal functioning of neurons in the olfactory bulb. The MNP agglomerates also did not disrupt the dense connections between the neurons in this

region. Since it is known that MNP chaining, and the resulting ability for magnetic fields to effectively move MNP through tissue[49–51] depend on particle properties (size, shape, concentration), in the future the studies above could be expanded to select optimal MNP properties to enable effective but safe MNP motion in the brain. Enabling safe and effective manipulation of MNPs in the brain would aid drug and gene delivery and other tissue engineering applications in the brain.

Appendix A. Supplementary data

Supplementary data to this article can be found online at http://dx.doi.org/10.1016/j.nano.2015.06.003.

References

1. Woodworth GF, Dunn GP, Nance EA, Hanes J, Brem H. Emerging insights into barriers to effective brain tumor therapeutics. *Front Oncol* 2014;**4**.
2. Dandy WE. Removal of right cerebral hemisphere for certain tumors with hemiplegia: preliminary report. *J Am Med Assoc* 1928;**90**:823-5.
3. Matsukado Y, Maccarty CS, Kernohan JW. The growth of glioblastoma multiforme (astrocytomas, grades 3 and 4) in neurosurgical practice. *J Neurosurg* 1961;**18**:636-44.
4. Ghose AK, Viswanadhan VN, Wendoloski JJ. A knowledge-based approach in designing combinatorial or medicinal chemistry libraries for drug discovery. 1. A qualitative and quantitative characterization of known drug databases. *J Comb Chem* 1999;**1**:55-68.
5. Kaiser MG, Parsa AT, Fine RL, Hall JS, Chakrabarti I, Bruce JN. Tissue distribution and antitumor activity of topotecan delivered by intracerebral clysis in a rat glioma model. *Neurosurgery* 2000;**47**:1391-8 [discussion 1398–1399].
6. Brem H, Piantadosi S, Burger PC, Walker M, Selker R, Vick NA, et al. Placebo-controlled trial of safety and efficacy of intraoperative controlled delivery by biodegradable polymers of chemotherapy for recurrent gliomas. The Polymer-brain Tumor Treatment Group. *Lancet* 1995;**345**:1008-12.
7. Stupp R, Mason WP, van den Bent MJ, Weller M, Fisher B, Taphoorn MJB, et al. Radiotherapy plus concomitant and adjuvant temozolomide for glioblastoma. *N Engl J Med* 2005;**352**:987-96.

8. Chinot OL, Wick W, Mason W, Henriksson R, Saran F, Nishikawa R, et al. Bevacizumab plus radiotherapy–temozolomide for newly diagnosed glioblastoma. *N Engl J Med* 2014;**370**:709-22.

9. Arruebo M, Fernández-Pacheco R, Irusta S, Arbiol J, Ibarra MR, Santamaría J. Sustained release of doxorubicin from zeolite–magnetite nanocomposites prepared by mechanical activation. *Nanotechnology* 2006;**17**:4057-64.

10. Hassan EE, Gallo JM. Targeting anticancer drugs to the brain. I: enhanced brain delivery of oxantrazole following administration in magnetic cationic microspheres. *J Drug Target* 1993;**1**:7-14.

11. Lockman PR, Mumper RJ, Khan MA, Allen DD. Nanoparticle technology for drug delivery across the blood-brain barrier. *Drug Dev Ind Pharm* 2002;**28**:1-13.

12. Pardridge WM. Drug transport across the blood–brain barrier. *J Cereb Blood Flow Metab* 2012;**32**:1959-72.

13. Del Burgo LS, Hernández RM, Orive G, Pedraz JL. Nanotherapeutic approaches for brain cancer management. *Nanomedicine Nanotechnol Biol Med* 2014;**10**:905-19.

14. Maier-Hauff K, Rothe R, Scholz R, Gneveckow U, Wust P, Thiesen B, et al. Intracranial thermotherapy using magnetic nanoparticles combined with external beam radiotherapy: results of a feasibility study on patients with glioblastoma multiforme. *J Neurooncol* 2007;**81**:53-60.

15. Kong SD, Lee J, Ramachandran S, Eliceiri BP, Shubayev VI, Lal R, et al. Magnetic targeting of nanoparticles across the intact blood-brain barrier. *J Control Release* 2012;**164**:49-57.

16. Wankhede M, Bouras A, Kaluzova M, Hadjipanayis CG. Magnetic nanoparticles: an emerging technology for malignant brain tumor imaging and therapy. *Expert Rev Clin Pharmacol* 2012;**5**:173-86.

17. Van Landeghem FKH, Maier-Hauff K, Jordan A, Hoffmann K-T, Gneveckow U, Scholz R, et al. Post-mortem studies in glioblastoma patients treated with thermotherapy using magnetic nanoparticles. *Biomaterials* 2009;**30**:52-7.

18. Sensenig R, Sapir Y, MacDonald C, Cohen S, Polyak B. Magnetic nanoparticle-based approaches to locally target therapy and enhance tissue regeneration in vivo. *Nanomedicine* 2012;**7**:1425-42.

19. Carenza E, Barceló V, Morancho A, Levander L, Boada C, Laromaine A, et al. In vitro angiogenic performance and in vivo brain targeting of magnetized endothelial progenitor cells for neurorepair therapies. *Nanomedicine Nanotechnol Biol Med* 2014;**10**:225-34.

20. Zhan C, Li B, Hu L, Wei X, Feng L, Fu W, et al. Micelle-based brain-targeted drug delivery enabled by a nicotine acetylcholine receptor ligand. *Angew Chem Int Ed* 2011;**50**:5482-5.

21. Feng B, Tomizawa K, Michiue H, Miyatake S, Han X-J, et al. Delivery of sodium borocaptate to glioma cells using immunoliposome conjugated with anti-EGFR antibodies by ZZ-His. *Biomaterials* 2009;**30**:1746-55.

22. Wu X-X, Kakehi Y, Mizutani Y, Kamoto T, Kinoshita H, Isogawa Y, et al. Doxorubicin enhances TRAIL-induced apoptosis in prostate cancer. *Int J Oncol* 2002;**20**:949-54.

23. Yang C, Rait A, Pirollo KF, Dagata JA, Farkas N, Chang EH. Nanoimmunoliposome delivery of superparamagnetic iron oxide markedly enhances targeting and uptake in human cancer cells in vitro and in vivo. *Nanomedicine Nanotechnol Biol Med* 2008;**4**:318-29.

24. Nacev A, Beni C, Bruno O, Shapiro B. Magnetic nanoparticle transport within flowing blood and into surrounding tissue. *Nanomedicine* 2010;**5**:1459-66.

25. Huynh NT, Morille M, Bejaud J, Legras P, Vessieres A, Jaouen G, et al. Treatment of 9 L gliosarcoma in rats by ferrociphenol-loaded lipid nanocapsules based on a passive targeting strategy via the EPR effect. *Pharm Res* 2011;**28**:3189-98.

26. Salcedo E, Tran T, Ly X, Lopez R, Barbica C, Restrepo D, et al. Activity-dependent changes in cholinergic innervation of the mouse olfactory bulb. *PLoS One* 2011;**6**:e25441.

27. Erb RM. *Magnetic manipulation and assembly of multi-component particle suspensions*. Duke University; 2009.

28. Hamill OP, Marty A, Neher E, Sakmann B, Sigworth FJ. Improved patch-clamp techniques for high-resolution current recording from cells and cell-free membrane patches. *Pflugers Arch* 1981;**391**:85-100.

29. Galarreta M, Hestrin S. A network of fast-spiking cells in the neocortex connected by electrical synapses. *Nature* 1999;**402**:72-5.

30. Sakmann B, Neher E. *Single-channel recording*. New York: Springer; 2009.

31. Zimnik NC, Treadway T, Smith RS, Araneda RC. α(1A)-adrenergic regulation of inhibition in the olfactory bulb. *J Physiol* 2013;**591**: 1631-43.

32. Shipley MT, Ennis M. Functional organization of olfactory system. *J Neurobiol* 1996;**30**:123-76.

33. Rye DB, Wainer BH, Mesulam M-M, Mufson EJ, Saper CB. Cortical projections arising from the basal forebrain: a study of cholinergic and noncholinergic components employing combined retrograde tracing and immunohistochemical localization of choline acetyltransferase. *Neuroscience* 1984;**13**:627-43.

34. Richter H, Wiekhorst F, Schwarz K, Lyer S, Tietze R, Alexiou C, et al. Magnetorelaxometric quantification of magnetic nanoparticles in an artery model after ex vivo magnetic drug targeting. *Phys Med Biol* 2009;**54**:N417-24.

35. Wang H, Su W, Wang S, Wang X, Liao Z, Kang C, et al. Smart multifunctional core–shell nanospheres with drug and gene co-loaded for enhancing the therapeutic effect in a rat intracranial tumor model. *Nanoscale* 2012;**4**:6501-8.

36. Ang D, Nguyen QV, Kayal S, Preiser PR, Rawat RS, Ramanujan RV. Insights into the mechanism of magnetic particle assisted gene delivery. *Acta Biomater* 2011;**7**:1319-26.

37. Jones GA, Niedoba H. IMP-field induced agglomeration in thin films of aqueous based magnetic fluids. *J Magn Magn Mater* 1988;**73**:33-8.

38. Domínguez-García P, Melle S, Pastor JM, Rubio MA. Scaling in the aggregation dynamics of a magnetorheological fluid. *Phys Rev E* 2007;**76**:051403.

39. Helgesen G, Skjeltorp AT, Mors PM, Botet R, Jullien R. Aggregation of magnetic microspheres: experiments and simulations. *Phys Rev Lett* 1988;**61**:1736-9.

40. Černák J, Helgesen G, Skjeltorp AT. Aggregation dynamics of nonmagnetic particles in a ferrofluid. *Phys Rev E* 2004;**70**:031504.

41. Vicsek T, Family F. Dynamic scaling for aggregation of clusters. *Phys Rev Lett* 1984;**52**:1669-72.

42. Witten TA, Sander LM. Diffusion-limited aggregation, a kinetic critical phenomenon. *Phys Rev Lett* 1981;**47**:1400-3.

43. Miyazima S, Meakin P, Family F. Aggregation of oriented anisotropic particles. *Phys Rev A* 1987;**36**:1421-7.

44. Erb RM, Sebba DS, Lazarides AA, Yellen BB. Magnetic field induced concentration gradients in magnetic nanoparticle suspensions: theory and experiment. *J Appl Phys* 2008;**103** [063916–063916–5].

45. Vartholomeos P, Mavroidis C. In silico studies of magnetic microparticle aggregations in fluid environments for MRI-guided drug delivery. *IEEE Trans Biomed Eng* 2012;**59**:3028-38.

46. Socoliuc V, Bica D, Vekas L. Estimation of magnetic particle clustering in magnetic fluids from static magnetization experiments. *J Colloid Interface Sci* 2003;**264**:141-7.

47. Kim JS, Yoon T-J, Yu KN, Kim BG, Park SJ, Kim HW, et al. Toxicity and tissue distribution of magnetic nanoparticles in mice. *Toxicol Sci* 2006;**89**:338-47.

48. Talelli M, Oliveira S, Rijcken CJF, Pieters EHE, Etrych T, Ulbrich K, et al. Intrinsically active nanobody-modified polymeric micelles for tumor-targeted combination therapy. *Biomaterials* 2013;**34**:1255-60.

49. Alexiou C, Arnold W, Klein RJ, Parak FG, Hulin P, Bergemann C, et al. Locoregional cancer treatment with magnetic drug targeting. *Cancer Res* 2000;**60**:6641-8.

50. Nacev A, Komaee A, Sarwar A, Probst R, Kim SH, Emmert-Buck M, et al. Towards control of magnetic fluids in patients: directing therapeutic nanoparticles to disease locations. *IEEE Control Syst* 2012;**32**:32-74.

51. Probst R, Lin J, Komaee A, Nacev A, Cummins Z, Shapiro B. Planar steering of a single ferrofluid drop by optimal minimum power dynamic feedback control of four electromagnets at a distance. *J Magn Magn Mater* 2011;**323**:885-96.